

# Tagged Neutron, Anti-neutron and $K_L^0$ beams in an Upgraded MIPP Spectrometer

Rajendran Raja<sup>1</sup>

<sup>1</sup> *Fermi National Accelerator laboratory*

*Batavia, IL 60510*

(Dated: May 23, 2006)

## Abstract

The MIPP experiment operating with an upgraded data acquisition system will be capable of acquiring data at the rate of 3000 events per second. Currently we are limited to a rate of 30 Hz due to the bottlenecks in the data acquisition electronics of the Time Projection Chamber (TPC). With the speeded up DAQ, MIPP will be capable of acquiring data at the rate of  $\approx$ 5 million events per day. This assumes a conservative beam duty cycle of 4 sec spill every 2 minutes with a 42% downtime for main injector beam manipulations for the  $\bar{p}$  source. We show that such a setup is capable of producing tagged neutron, anti-neutron and  $K_L^0$  beams that are produced in the MIPP cryogenic hydrogen target using proton, anti-proton and  $K^\pm$  beams. These tagged beams can be used to study calorimeter responses for use in studies involving the Particle Flow Algorithm (PFA). The energy of these tagged beams will be known to better than 2% on a particle by particle level by means of constrained fitting. We expect a tagged beam rate in the tens of thousands a day. The MIPP spectrometer thus offers a unique opportunity to study the response of calorimeters to neutral particles.

## I. INTRODUCTION

The MIPP experiment at Fermilab is an open geometry spectrometer [1] designed to study non-perturbative QCD interactions on a variety of nuclear targets including liquid hydrogen. It has just completed its first run using a time projection chamber (TPC) that currently takes data at  $\approx 30\text{Hz}$ . Beams of  $\pi^\pm, K^\pm$  and  $p^\pm$  from a momentum range 5 GeV/c-85 GeV/c have been obtained using the secondary beamline designed by MIPP. The experiment has very nearly complete acceptance of all forward going charged particles and particle identification is performed using  $dE/dx$  (in the TPC), time of flight, multi-cell Cerenkov and a RICH counter that provides  $3\sigma$  separation between  $\pi, K$  and  $p$  hypotheses over nearly all of accepted phase space. A schematic of the spectrometer is shown in Figure 1.

With an upgraded data acquisition system, MIPP can be made to take data at 3000Hz. Details of the MIPP upgrade which is estimated to cost less than \$500,000 may be found in reference [2].

### A. The Beamline

The secondary beamline is shown in Figure 2. The beamline in an upgraded mode will be capable of delivering charged kaons down to 3 GeV/c and charged pions protons and anti-protons down to 1 GeV/c. This excellent performance of the beam is due to the relatively short distance of 90 meters from the primary production target to the secondary target. The other constraints on the beam are that the primary target be focused on the momentum selection collimator which should be in an area of dispersion so that the momentum bite  $\delta p/p$  of the beam can be controlled by opening the collimator. The collimator is usually set so that  $\delta p/p = 0.02$ . The other constraint on the beamline is that the divergence of the beam is small ( $< 0.3 \text{ mr}$ ) in the region of the beam Cerenkovs. The MIPP beamline design was selected from a set of 6 different designs after a great deal of design activity. More details of the beam may be found in reference [3]. The beam particle is identified by two differential Cerenkovs for particles above  $\approx 10 \text{ GeV}/c$  momentum and by a time of flight system for particles below this. The particle identification trigger is “anded” with the minimum bias interaction trigger to provide the experimental trigger. The composition of the beam depends on the beam momentum. In order to obtain equal number of interactions

# MIPP

## Main Injector Particle Production Experiment (FNAL-E907)

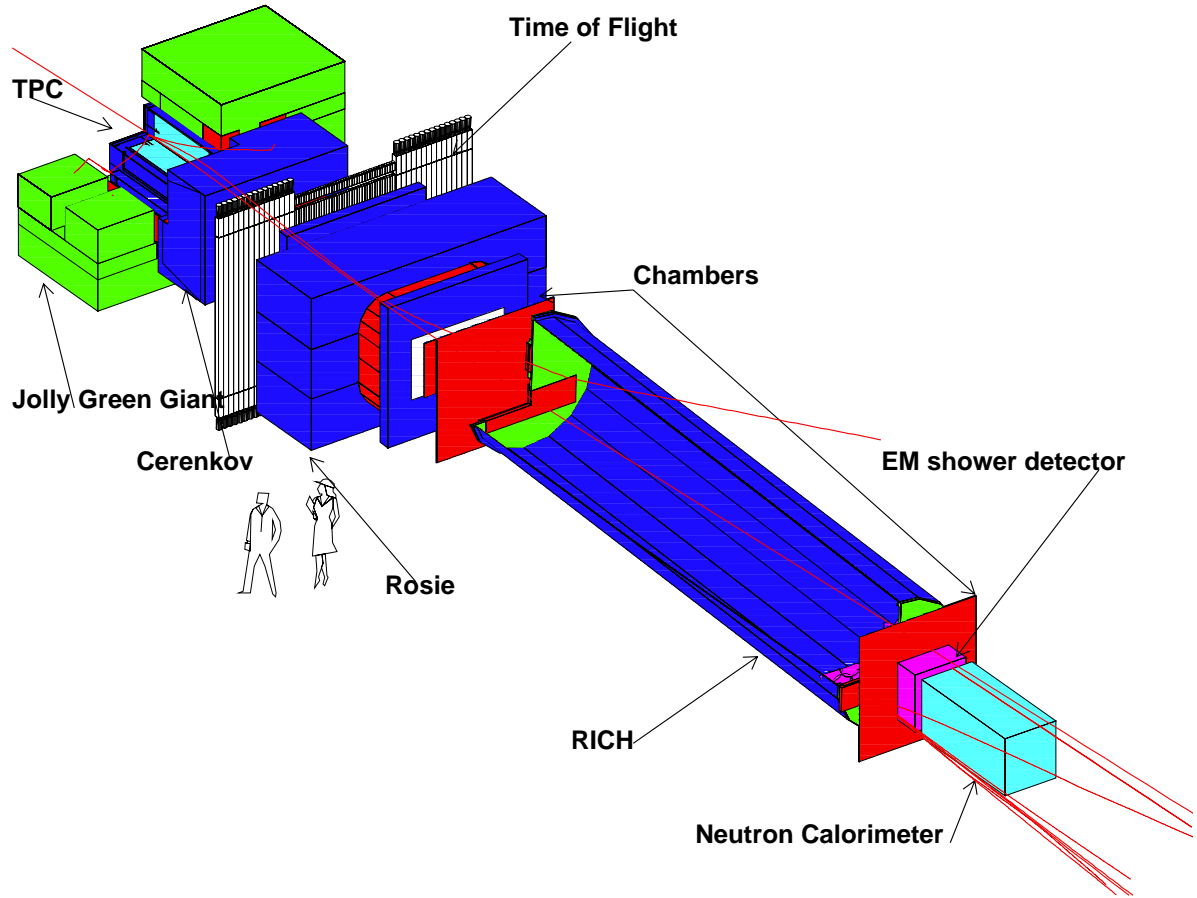


FIG. 1: A Geant3 based view of the MIPP Spectrometer. The electromagnetic and neutron calorimeters can be replaced by an ILC test calorimeter to study the response to tagged neutron and  $K_L^0$  beams with an upgraded MIPP spectrometer

for all three particle species, the beam triggers are prescaled by the appropriate amounts that depend on the beam momentum.

## MIPP BEAM

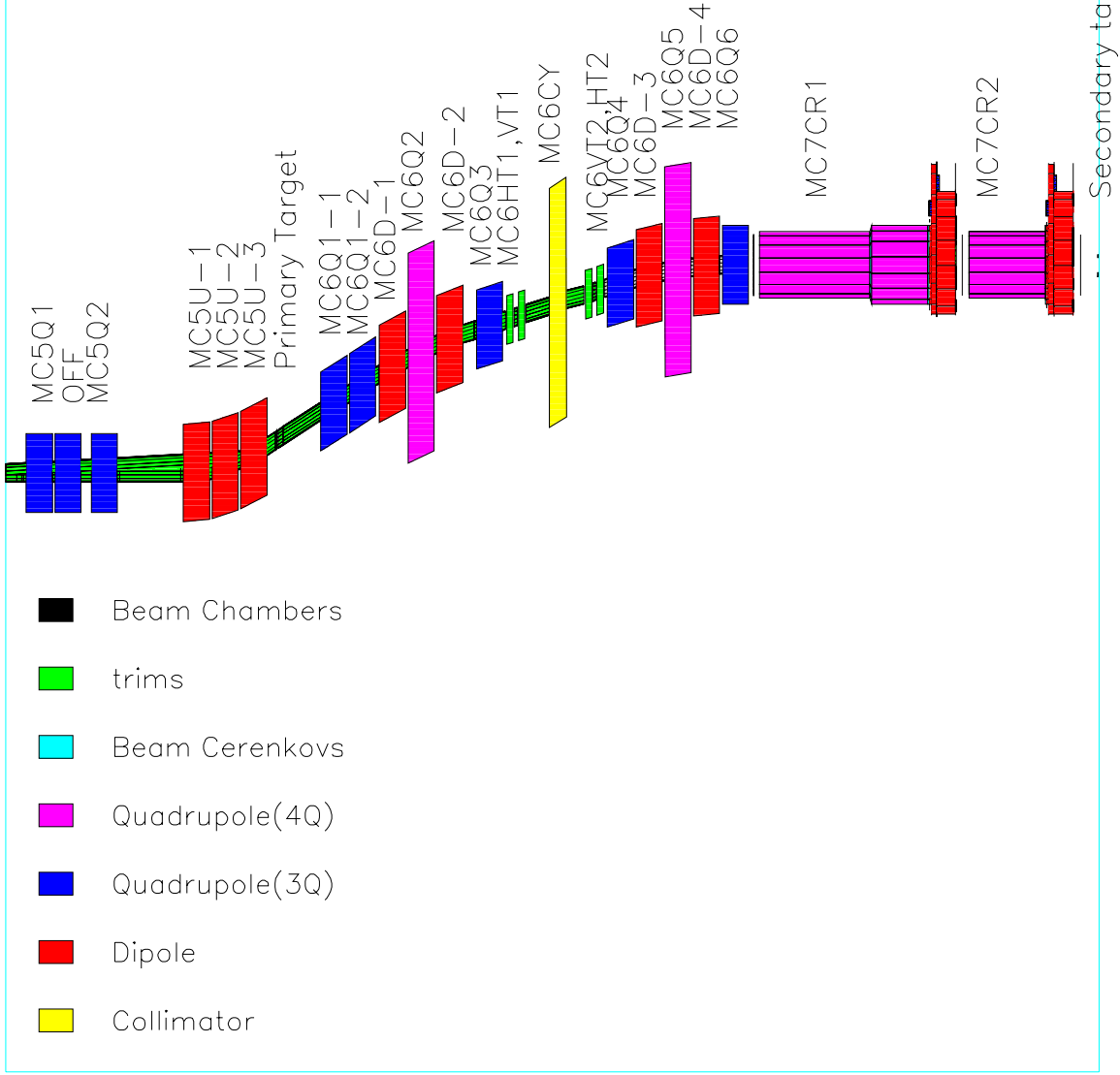


FIG. 2: The MIPP secondary beamline.

### B. Cryogenic Target

The tagged neutron, anti-neutron and  $K_L^0$  beams require the use of constrained fitting, which make use of the energy momentum constraints at the primary vertex. This requires that the scattering take place on a proton target. Nuclear targets will produce many undetected neutrals which make constrained fitting next to impossible. The physics being proposed here can thus only be done using a liquid hydrogen target. In the first MIPP run,

we operated a cryogenic target that functioned very well. Figure 3 shows the target installed and operating in the TPC bay. For a summary of the physics channels available using a hydrogen target, please see ref [4].



FIG. 3: The MIPP cryogenic target filled with liquid hydrogen operating in the TPC bay during the first MIPP run.

## II. DIFFRACTIVE REACTIONS

The physics that makes tagged neutral beams possible can be summarized in one sentence— Diffractive beam fragmentation in a hydrogen target.

The reactions in question are



These reactions can be picturized by the exchange diagrams shown in figure 4. Diffractive reactions, being due to Pomeron exchange fall relatively slowly with incident beam momentum as opposed to pure charge exchange reactions.

### A. Constrained Fitting

The art of constrained fitting was used extensively during the hey-dey of the bubble chamber whereby it was used to separate various exclusive reactions from each other. The program SQUAW is an example of many such computer programs that minimized a  $\chi^2$  to obtain fitted four-vectors of the particles in the reaction allowing for the measurement errors and correlations. In a reaction where the beam momentum 4-vector is assumed known (MIPP identifies the beam particle using beam Cerenkovs and the beam track is measured using the beam chambers. The beam momentum is known to  $\approx 2\%$ ), and the target particle can be reliably assumed to be a proton, and all the final state particles are identified, one can apply the conservation of energy and momentum to produce a fit with 4 constraints. Such a fit is known in the jargon as a 4-C fit. If the final state momenta are measured accurately, then reactions with missing neutrals will in general tend not to fit. When one of the final state particles is a missing neutral, the three momentum of the missing neutral is unknown. The fitting hypothesis assigns a mass to the missing neutral, and this produces a 1-C fit. For the reactions we study here, a missing neutron,  $\bar{n}$  or  $K_L^0$  will thus result in a 1-C fit. If the neutral is observed in the calorimeter and its point of impact is measured to some accuracy (e.g a measurement error in neutral position of 20 cm transversely will result in an error in neutral direction of 8mr, with the calorimeter at its present position ), one obtains a 3-C fit. Such 3-C fits are constrained enough to reject events with further missing  $\pi^0$ 's, resulting in a fitted momentum of the  $n, \bar{n}$  or  $K_L^0$  that is known to  $\approx 2\%$ . This fitted momentum can then be compared to the measured momentum in the calorimeter to study

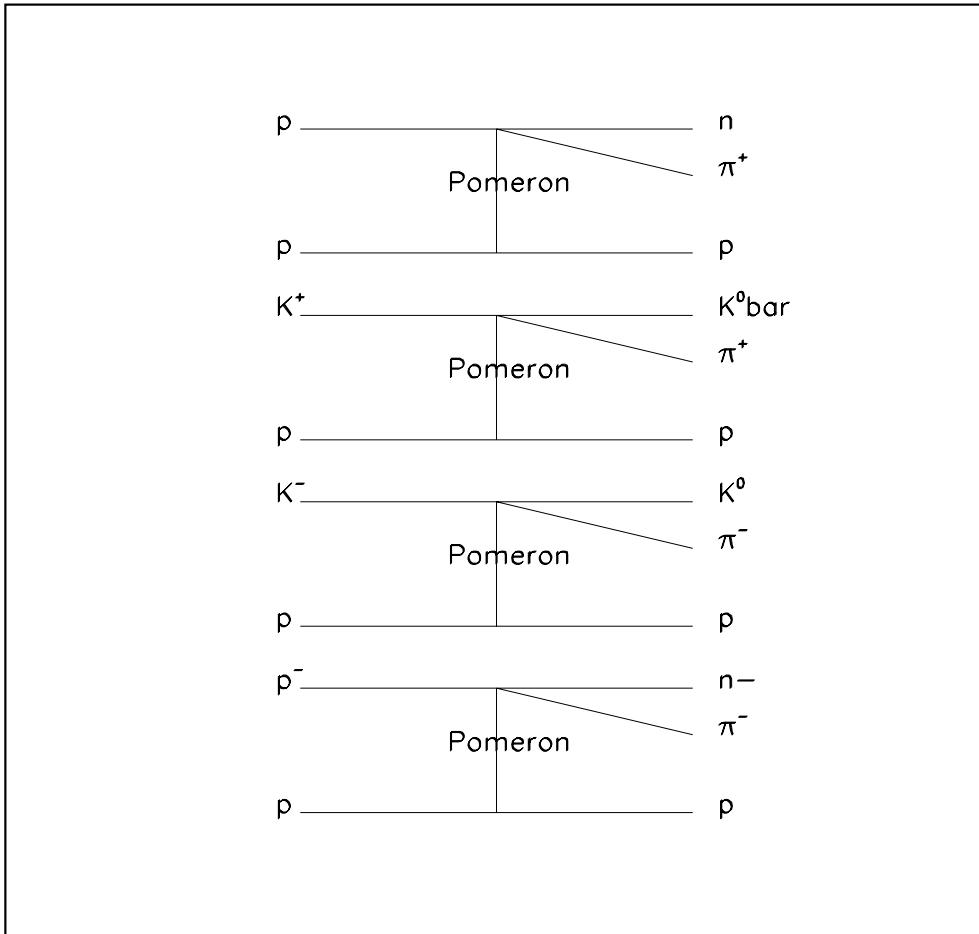


FIG. 4: The diffractive diagrams illustrating beam fragmentation for proton, kaon and anti-proton beams. A pomeron is exchanged causing the beam to fragment. In the proton case, there is a symmetric target fragmentation diagram which will cause the emission of slow neutrons and pions from the target with the beam remaining intact. These neutrons will be lost .

the calorimeter response and linearity. The transverse size of the neutral shower can be studied as a function of the neutral particle momentum.

It is worth noting that the quality of the 3-C fit improves as the direction of the missing neutral is known better. For this, placing the calorimeter farther away from the cryotarget improves the precision of the missing neutral direction. Since the neutral beam is the result of beam diffraction, the loss in acceptance is much less than the inverse square of the distance from the interaction point.

### III. MONTE CARLO GENERATION

The program DPMJET was used [5] to generate the reactions  $pp \rightarrow X$ ,  $K^+p \rightarrow X$ ,  $K^-p \rightarrow X$  and  $\bar{p}p \rightarrow X$ . We generated samples of  $10^5$  events for  $pp$  interactions at beam momenta of 10,20,30,60 and 90 GeV/c. Even though MIPP has run with  $K^-$  beams of 85 GeV/c, the prescale factors are large.  $K^+$  beams above 60 GeV/c become problematic, because the proton flux is large. So we do not generate the 90 GeV/c point for kaon beams. For the kaon beams, we generate 200,000 events each, since the relative DPMJET cross section seems lower for diffraction in  $K^\pm p$  events. We have generated 100,000 events for  $\bar{p}p$  interactions at beam momenta of 10,20,30 and 60 GeV/c.

#### A. Acceptance criteria

The MIPP calorimeter entrance plane is placed at a distance of 2458.6 cm from the center of the MIPP liquid hydrogen target volume. If the neutral particle in the event impacts the calorimeter within a radius of 75 cm from the beam axis, that neutral particle is considered accepted for the purposes of this simulation. Similarly a slow proton of momentum 0.206 GeV/c has a range of 10 cm in liquid hydrogen. if the slow proton is more energetic than this, we accept the event. The length in the beam direction of the target flask is 10.48 cm in length along the beam direction. So on average, these protons should make it out of the hydrogen and into the TPC. MIPP upgrade also plans to have a recoil detector around the target, to detect wide angle slow protons.

## B. Calculated event rates

We assume a spill of 4 seconds duration every 2 minutes. We assume a DAQ rate of 3000 events per second during the spill. We assume the machine is delivering beam 58% of the time, the rest being devoted to anti-proton stacking manipulations. These numbers are conservative. Under these assumptions, MIPP should be able to log 5 millions events/day to disk. The events of interest will be among these. The events where the hadron calorimeter has significant neutral energy can be used to flag and filter these events for faster offline processing.

In what follows, we calculate the events obtainable /day assuming the total bandwidth is dedicated to the trigger in question. In practice, we would select the charge of the beam and prescale the proton, kaon and anti-proton beams as required.

## IV. RESULTS

Table I lists the inelastic cross sections of DPMJET generated events for  $pp$ ,  $K^+p$ ,  $K^-p$  and  $\bar{p}p$  events and compares them to known data obtained from PDG listings. Table II lists the mean charged multiplicities of DPMJET generated events and compares them to data. The data multiplicities were estimated by a fit of the form  $\langle n \rangle = a + b\ln(E_a) + c\ln^2(E_a)$ , where  $E_a$  is the available energy in the collision defined as  $E_a = \sqrt{s} - m_{beam} - m_{target}$ , and  $a=2.45$ ,  $b=0.32$  and  $c=0.53$ . See ref [8]. DPMJET does a reasonable job at estimating the  $pp$  total inelastic cross section and mean multiplicity as a function of center of mass energy. It seems to overestimate the  $K^\pm p$  inelastic cross sections.

### A. The reaction $pp \rightarrow n\pi^+p$

Figure 5 shows the cross section of  $pp \rightarrow pn\pi^+$  events as a function of beam momentum and compares them to the other diffractive channels  $np \rightarrow pp\pi^-$  and  $pp \rightarrow pp\pi^0$ . This plot is taken from my thesis experiment [6] which was on the channel  $np \rightarrow pp\pi^-$ . Some of the cross section points for the channel  $np \rightarrow pp\pi^-$  were determined by a technique that used “tagged neutrons” by observing  $np$  elastic scattering in the bubble chamber followed by the neutron re-interacting in the chamber [7], which determines the neutron spectra.

Figure 6 shows the angle of the neutron for this reaction as a function of the neutron

Beam Momentum	pp inelastic		$K^+ p$ inelastic		$K^- p$ inelastic	
	(mb)		(mb)		(mb)	
GeV/c	DPMJET	data	DPMJET	data	DPMJET	data
10	32.29	30.0	21.05	13.96	22.09	19.96
20	31.67	30.06	20.43	14.22	21.41	18.28
30	31.55	30.89	20.24	15.33	21.13	18.28
60	31.63	31.84	20.13	16.07	20.83	17.70
90	31.84	30.50	-	16.12	-	17.29

TABLE I: Comparison of inelastic cross sections generated by DPMJET to data

TABLE II: Comparison of mean charge multiplicities generated by DPMJET to data

Beam Momentum	pp inelastic		$K^+ p$ inelastic		$K^- p$ inelastic	
	multiplicity		multiplicity		multiplicity	
GeV/c	DPMJET	data	DPMJET	data	DPMJET	data
10	3.70	3.27	3.97	3.45	3.59	3.45
20	4.66	4.09	4.93	4.25	4.68	4.25
30	5.27	4.62	5.52	4.77	5.32	4.77
60	6.34	5.66	6.59	5.77	6.45	5.77
90	7.04	6.31	-	6.42	-	6.42

momentum for an incident proton beam momentum of 90 GeV/c. The wide angle neutrons are a result of target fragmentation. The beam diffraction events have the neutron at a small angle heading straight for the calorimeter, irrespective of the neutron momentum. The acceptance of these neutrons is not increased by bringing the calorimeter closer. However, the precision to which the neutron 4-vector is known increases linearly as the calorimeter is placed farther away from the interaction point, due to a better measurement of the neutron angles. Table III tabulates the results of the DPMJET simulation. The cross section for the process  $pp \rightarrow pn\pi^+$  as calculated by DPMJET is lower than the data by a factor of 3-4. This graphically illustrates the problem of hadronic physics simulators. If we use the data cross sections, we obtain 47,069 tagged neutrons in a calorimeter with a 60 GeV/c proton

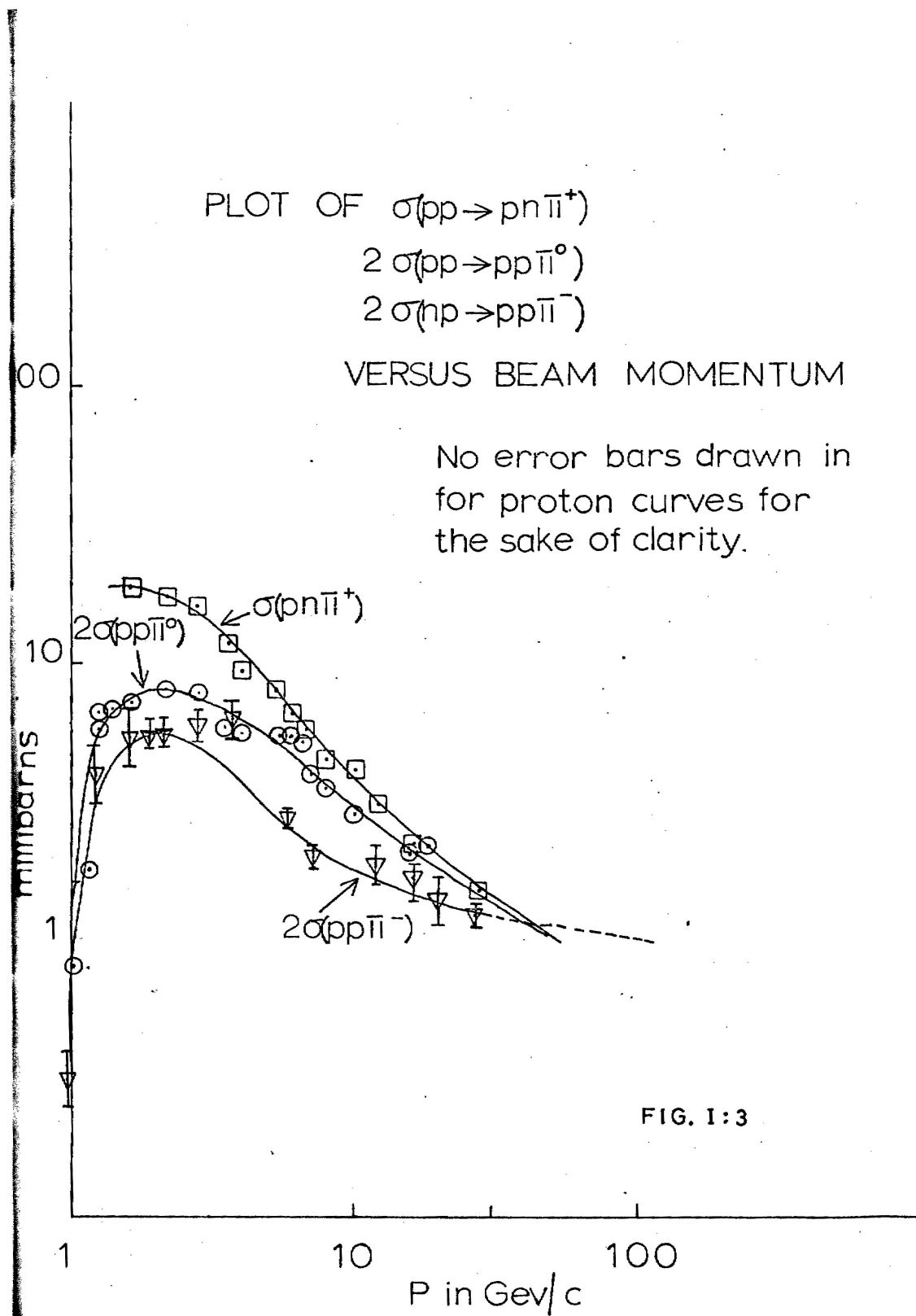


FIG. 5: The experimentally measured cross section for the reaction  $pp \rightarrow pn\pi^+$  compared with similar diffractive processes.

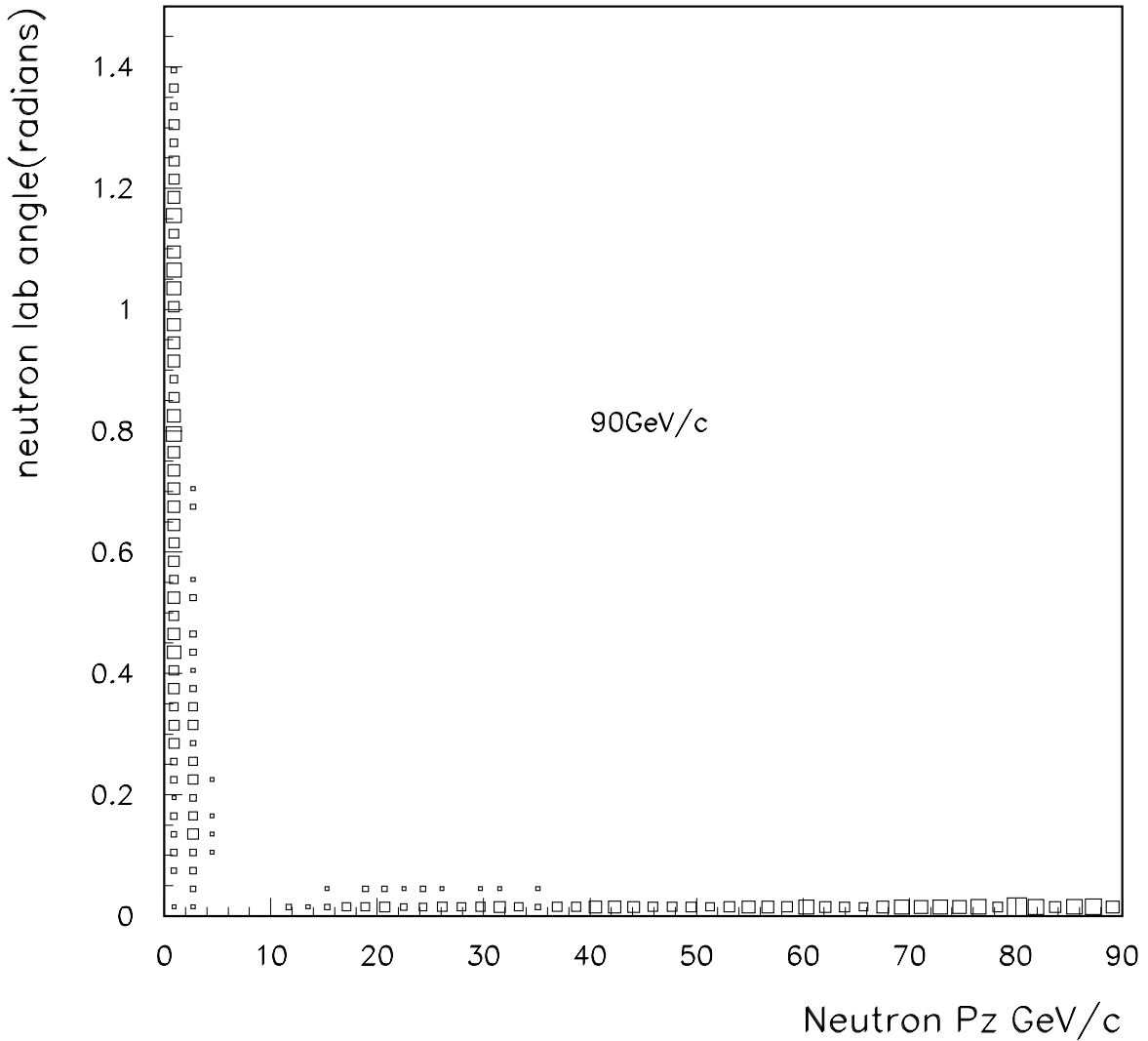


FIG. 6: The lab angle of the neutron as a function of the neutron momentum for the reaction  $pp \rightarrow pn\pi^+$  for a beam momentum of 90 GeV/c. The wide angle neutrons are the result of target fragmentation.

beam. DPMJET evaluates this rate as being 16,250. There are very few additional data points in this channel since 1975, the time of my thesis. This fact alone accentuates our lack of knowledge of hadronic physics and the urgent need for accurate high statistics data which the MIPP upgrade can provide. Figures 7, 8 and 9 show the neutron, proton and

TABLE III: Expected number of events/day using the DPMJET and data cross sections for the process  $pp \rightarrow pn\pi^+$ . DPMJET underestimates the cross section.

Beam Momentum	dpmjet	data	dpmjet	accepted	dpmjet	data
GeV/c	mb	mb	generated	events	events/day	events/day
10	1.373	3.880	4252	135	6750	20532
20	0.409	1.970	1290	207	10350	52581
30	0.345	1.429	1092	314	15700	66511
60	0.280	0.816	885	325	16250	47069
90	0.255	0.638	801	288	14400	37600

pion spectra of accepted events as a function of beam momentum.

### B. The reaction $K^+p \rightarrow K_L^0\pi^+p$

Table IV tabulates the DPMJET cross section for the process  $K^+p \rightarrow pK_L^0\pi^+$ . We have not attempted to compare the DPMJET cross sections to data cross sections, though the agreement in this channel may be better than in the  $pp$  case. Figures 10, 11 and 12 show the momentum spectra of  $K_L^0$ , proton and pions in the accepted events, as a function of beam momenta.

TABLE IV: Expected number of events/day using the DPMJET for the process  $K^+p \rightarrow pK_L^0\pi^+$ .

Beam Momentum	dpmjet	dpmjet	dpmjet	accepted	dpmjet
GeV/c	inel. mb	mb	generated	events	events/day
10	21.05	0.226	2152	176	4400
20	20.43	0.113	1110	360	9000
30	20.24	0.093	923	495	12375
60	20.13	0.086	855	630	15750

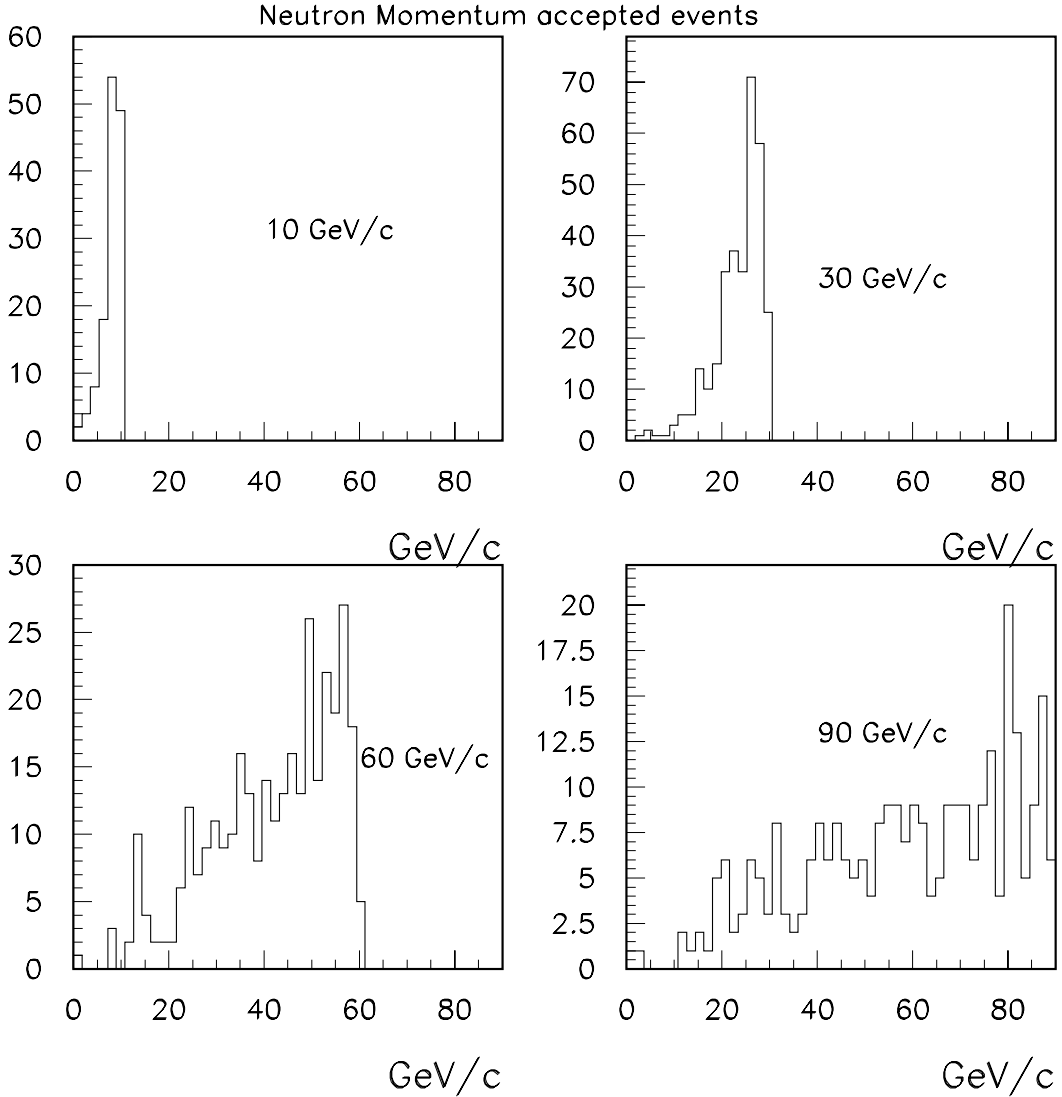


FIG. 7: Momentum spectrum of accepted neutrons for incident proton momenta of 10 GeV/c, 30 GeV/c, 60 GeV/c and 90 GeV/c for the process  $pp \rightarrow pn\pi^+$ .

### C. The reaction $K^- p \rightarrow K_L^0 \pi^- p$

Table V tabulates the DPMJET cross section for the process  $K^- p \rightarrow pK_L^0 \pi^-$ . We have again not attempted to compare the DPMJET cross sections to data cross sections, though the agreement in this channel may be better than in the  $pp$  case. Figures 13, 14 and 15 show the momentum spectra of  $K_L^0$ , proton and pions in the accepted events, as a function

2006/05/08 11.29

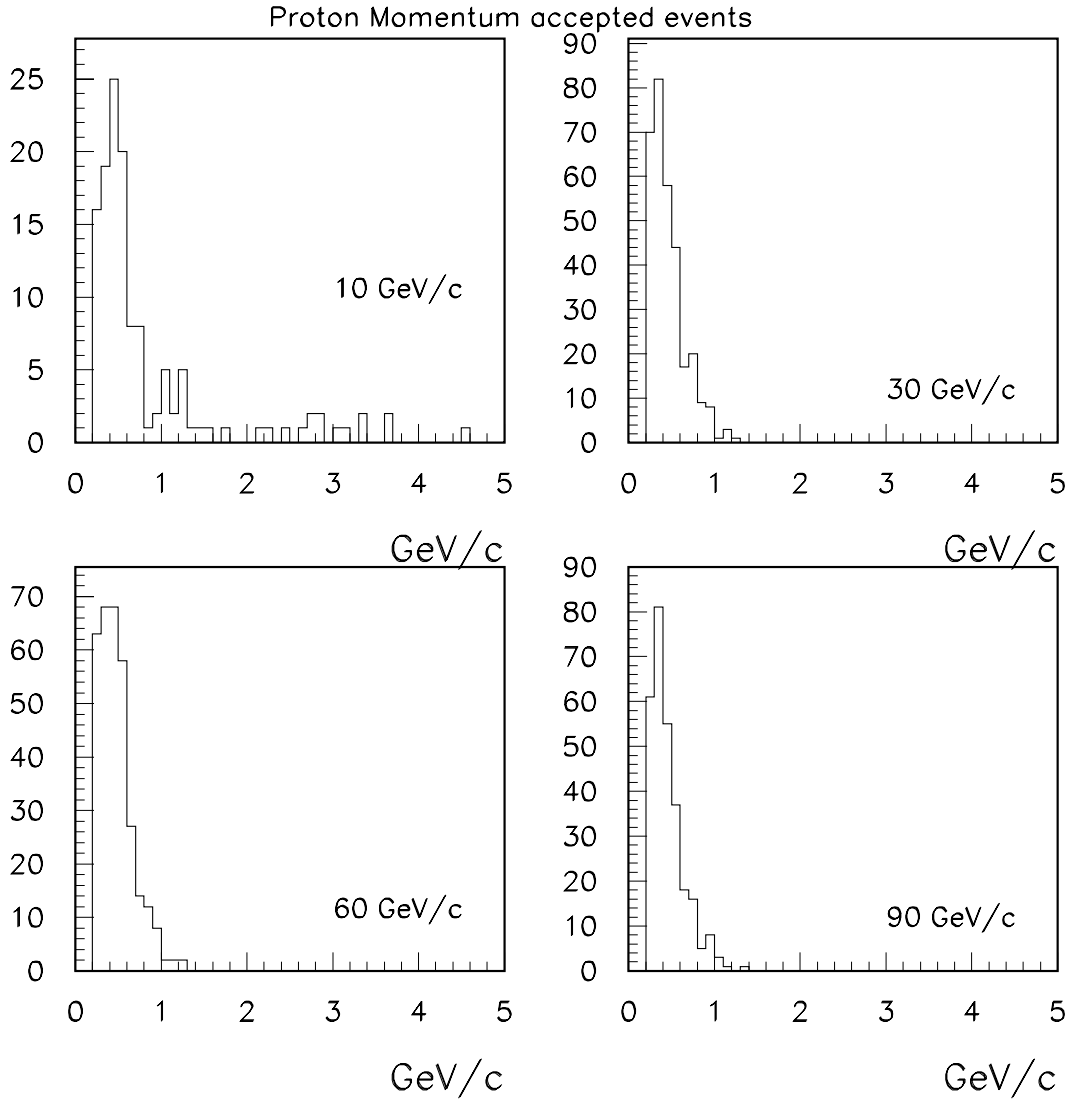


FIG. 8: Momentum spectrum of accepted protons for incident proton momenta of 10 GeV/c, 30 GeV/c, 60 GeV/c and 90 GeV/c for the process  $pp \rightarrow pn\pi^+$ .

of beam momenta.

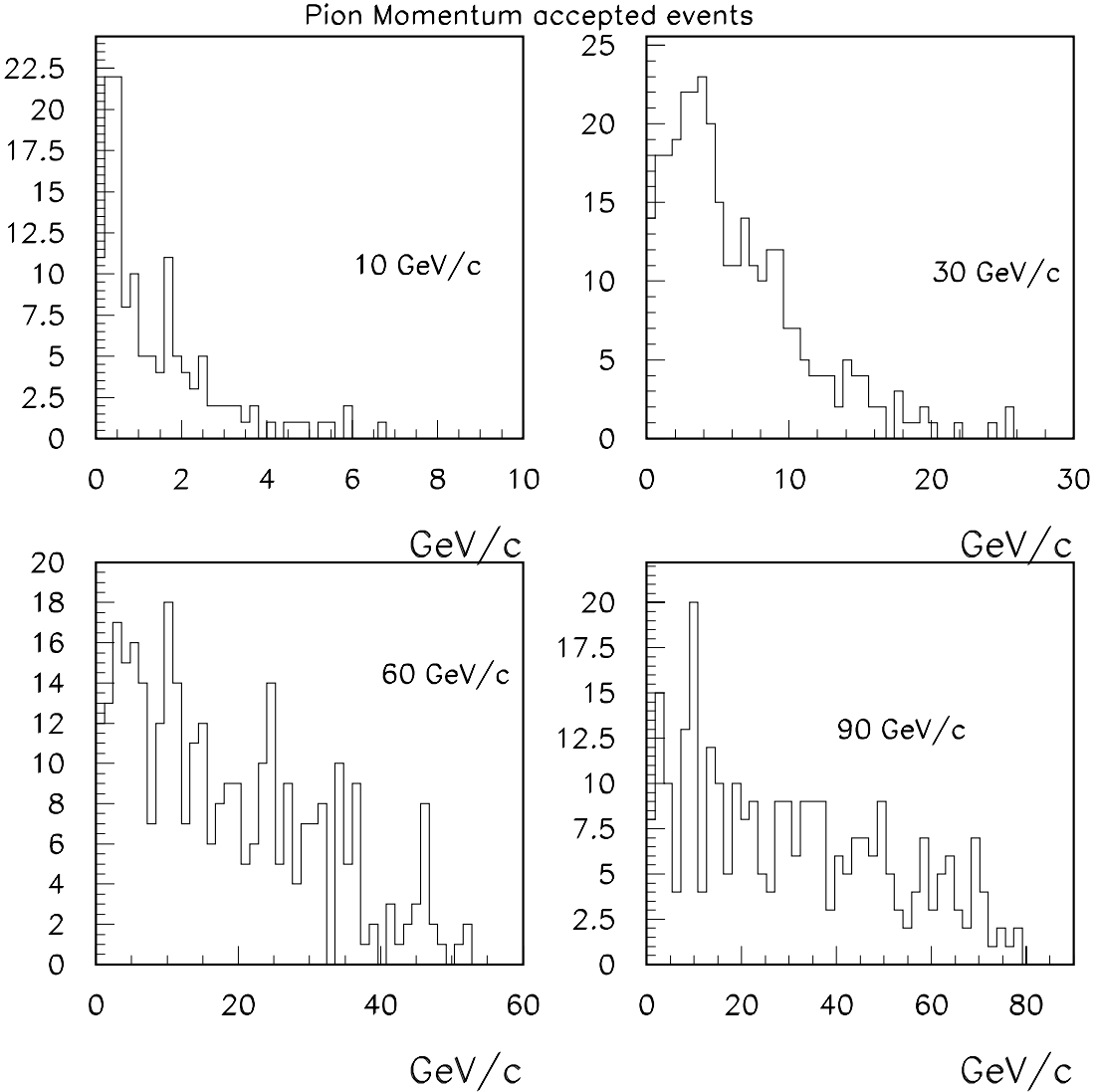


FIG. 9: Momentum spectrum of accepted  $\pi^+$  particles for incident proton momenta of 10 GeV/c, 30 GeV/c, 60 GeV/c and 90 GeV/c for the process  $pp \rightarrow pn\pi^+$ .

#### D. The reaction $\bar{p}p \rightarrow \bar{n}\pi^-p$

Table VI tabulates the results of the DPMJET simulation. We expect the same mismatch between the DPMJET cross sections and the data in this channel as in the  $pp$  case, though data are even sparser. We estimate the number of anti-neutrons expected as a function of

2006/05/09 15.55

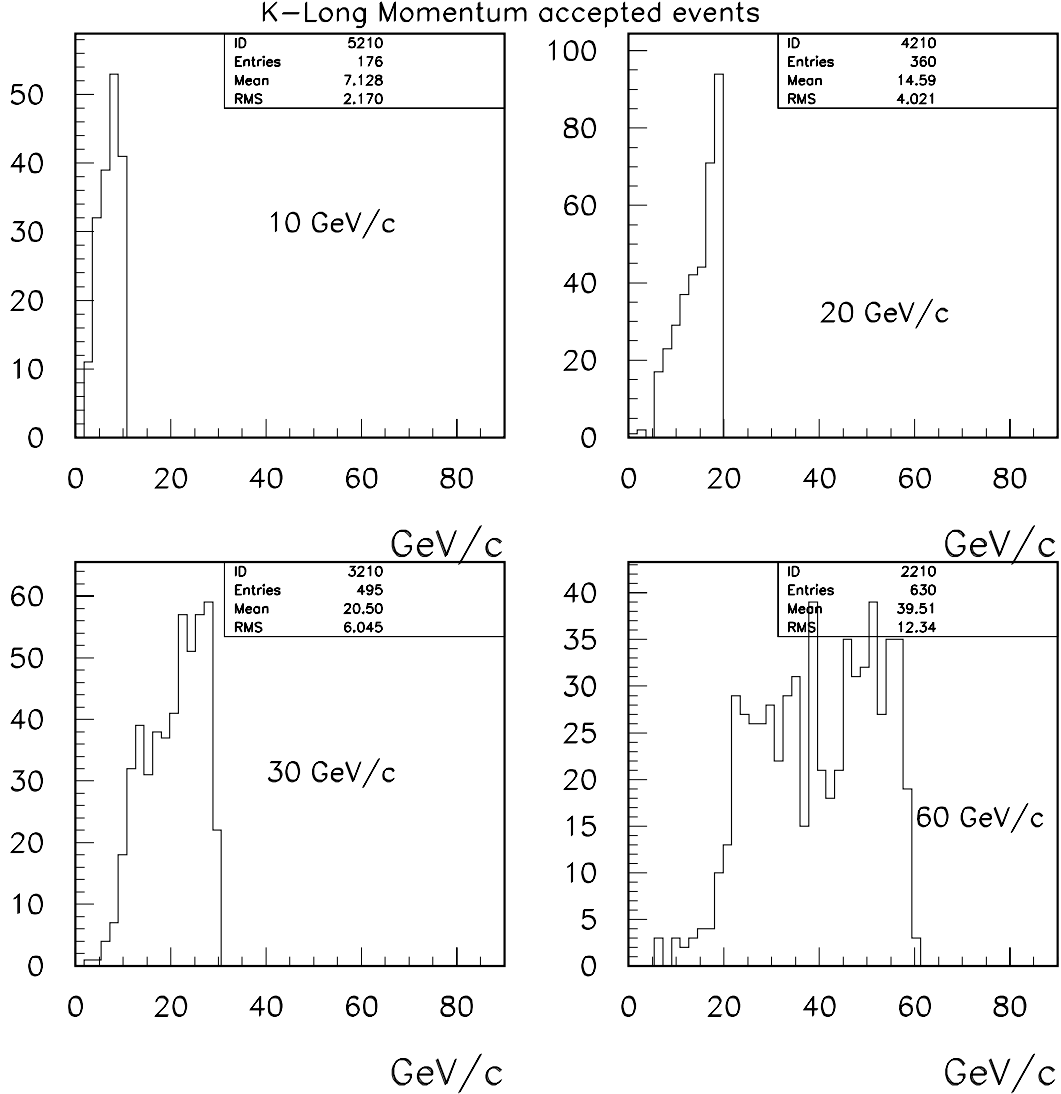


FIG. 10: Momentum spectrum of accepted  $K_L^0$  particles for incident  $K^+$  momenta of 10 GeV/c, 20 GeV/c, 30 GeV/c and 60 GeV/c for the process  $K^+ p \rightarrow p K_L^0 \pi^+$ .

beam momentum, with the proviso that the data may have higher rates by a factor of 3-4. Figures 16, 17 and 18 show the anti-neutron, proton and pion spectra of accepted events as a function of beam momentum.

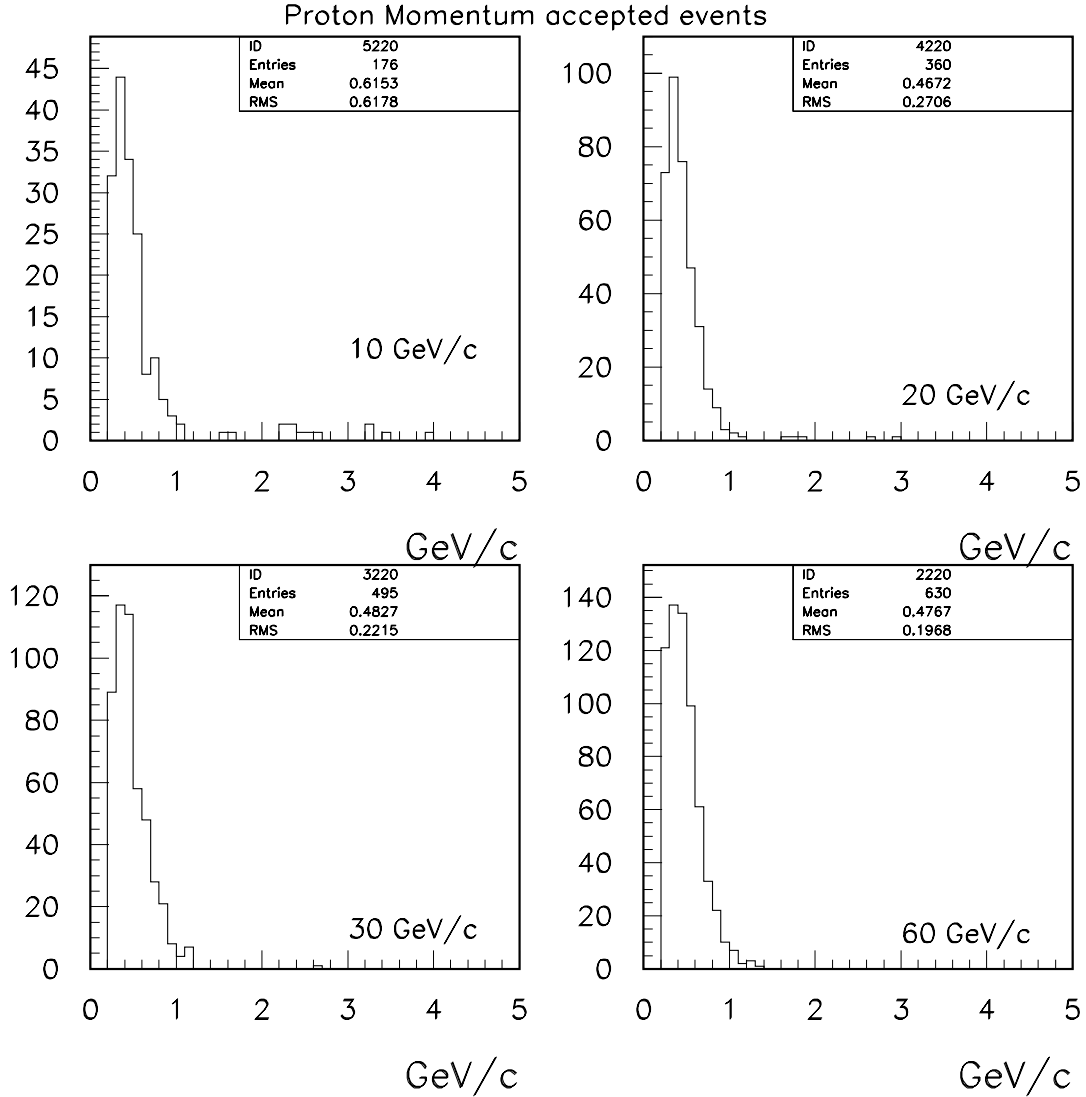


FIG. 11: Momentum spectrum of accepted protons for incident  $K^+$  momenta of 10  $\text{GeV}/c$ , 20  $\text{GeV}/c$ , 30  $\text{GeV}/c$  and 60  $\text{GeV}/c$  for the process  $K^+ p \rightarrow p K_L^0 \pi^+$ .

## V. CONCLUSIONS

We propose a scheme by which we obtain tagged neutron, anti-neutron and  $K_L^0$  beams using an upgraded MIPP spectrometer. A test calorimeter placed behind the RICH counter in MIPP will enable the study of neutral particle response in the calorimeter. The momenta

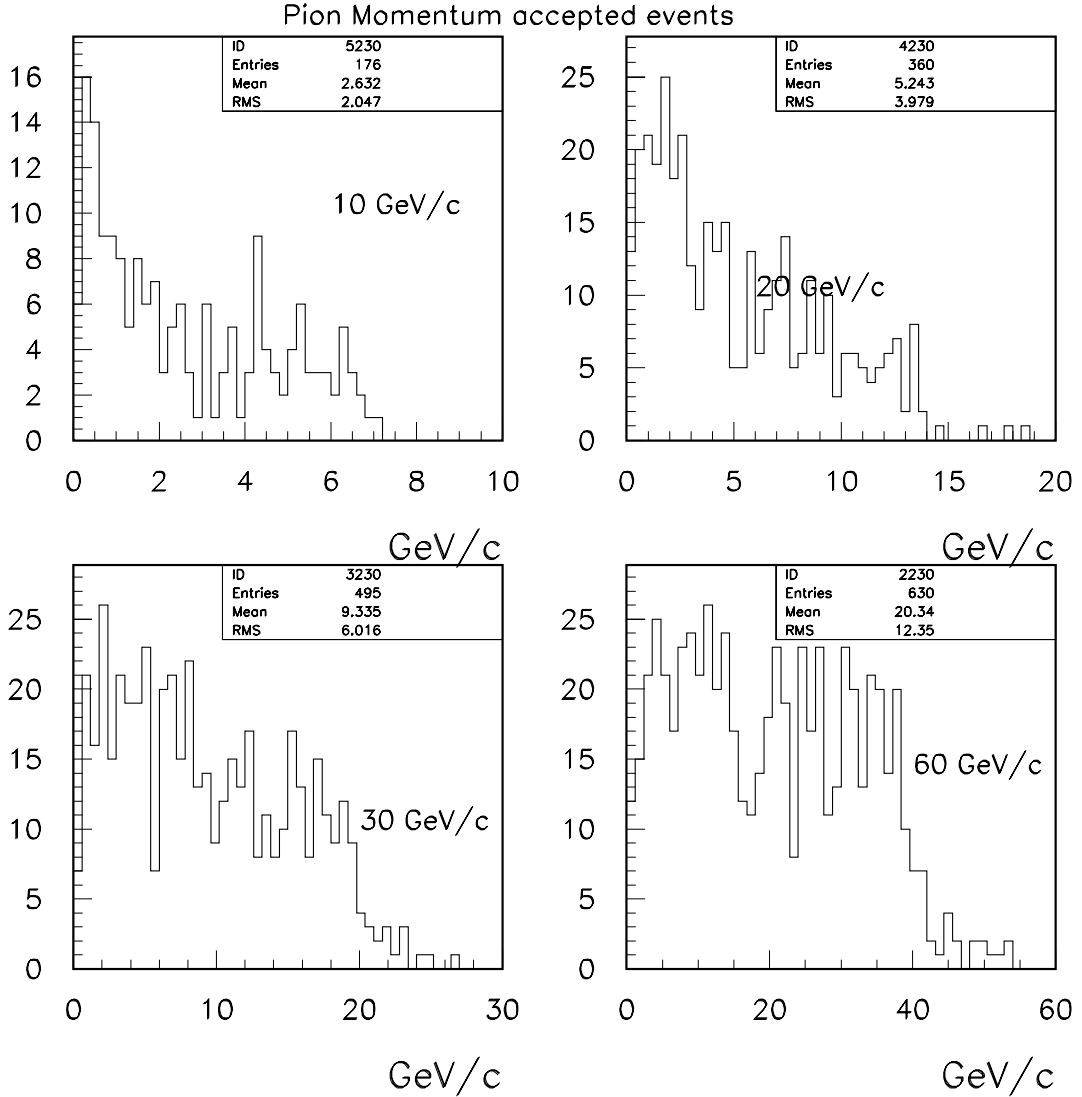


FIG. 12: Momentum spectrum of accepted  $\pi^+$  particles for incident  $K^+$  momenta of 10  $\text{GeV}/c$ , 20  $\text{GeV}/c$ , 30  $\text{GeV}/c$  and 60  $\text{GeV}/c$  for the process  $K^+ p \rightarrow p K_L^0 \pi^+$ .

of the tagged neutral particle will be known on a particle by particle basis to better than 2%. The upgraded MIPP calorimeter will also permit the acquisition of hadroproduction data on a number of nuclei of unprecedented quality and precision. Such data will dramatically improve our knowledge of QCD processes and our ability to simulate hadronic showers. We note in passing that the kaon tagging results in pure  $K^0$  and  $\bar{K}^0$  states at the

TABLE V: Expected number of events/day using the DPMJET for the process  $K^- p \rightarrow p K_L^0 \pi^-$ .

Beam Momentum	dpmjet	dpmjet	dpmjet	accepted	dpmjet
GeV/c	inel mb	mb	generated	events	events/day
10	22.09	0.178	1616	177	4425
20	21.41	0.120	1122	376	9400
30	21.13	0.105	993	567	14175
60	20.83	0.082	784	565	14125

TABLE VI: Expected number of events/day using the DPMJET for the process  $\bar{p}p \rightarrow p\bar{n}\pi^-$ .

Beam Momentum	dpmjet	dpmjet	dpmjet	accepted	dpmjet
GeV/c	inel. mb	mb	generated	events	events/day
10	40.63	0.223	1097	133	6650
20	38.08	0.108	568	229	11450
30	36.96	0.099	536	270	13500
60	35.60	0.068	381	271	13550

production vertex. The physics implications of this for possible CP-violation studies need to be investigated further.

- [1] Information on the MIPP Experiment may be found at

<http://ppd.fnal.gov/experiments/e907/>

The MIPP experiment proposal may be found at

<http://ppd.fnal.gov/experiments/e907/notes/MIPPnotes/public/pdf/MIPP0003/MIPP0003.pdf>

The addendum to the MIPP proposal may be found at

<http://ppd.fnal.gov/experiments/e907/notes/MIPPnotes/public/pdf/MIPP0004/MIPP0004.pdf>

- [2] “The MIPP Upgrade Document”,

<http://ppd.fnal.gov/experiments/e907/notes/MIPPnotes/public/pdf/MIPP0068/MIPP0068.pdf>

- [3] The MIPP beamline design paper was submitted to the PAC2003 conference. One can find a

2006/05/19 13.51

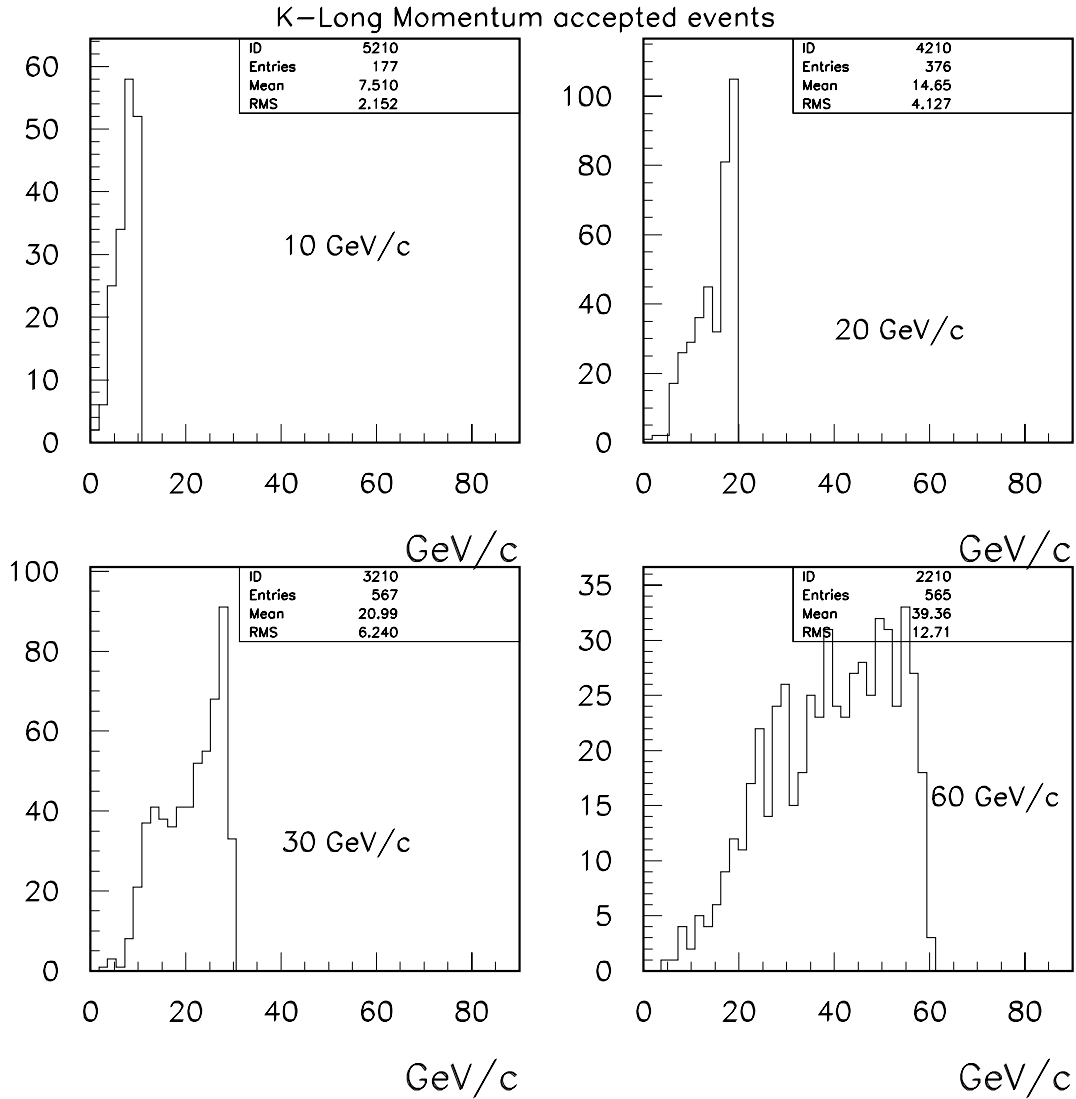


FIG. 13: Momentum spectrum of accepted  $K_L^0$  particles for incident  $K^-$  momenta of 10 GeV/c, 20 GeV/c, 30 GeV/c and 60 GeV/c for the process  $K^- p \rightarrow p K_L^0 \pi^-$ .

copy of the paper at

[http://ppd.fnal.gov/experiments/e907/Beam/mipp\\_beam\\_pac03.doc](http://ppd.fnal.gov/experiments/e907/Beam/mipp_beam_pac03.doc)

- [4] “Arguments for a Liquid Hydrogen Target in MIPP”, R.Raja,  
<http://ppd.fnal.gov/experiments/e907/notes/MIPPnotes/public/pdf/MIPP0010/MIPP0010.pdf>

2006/05/19 13.51

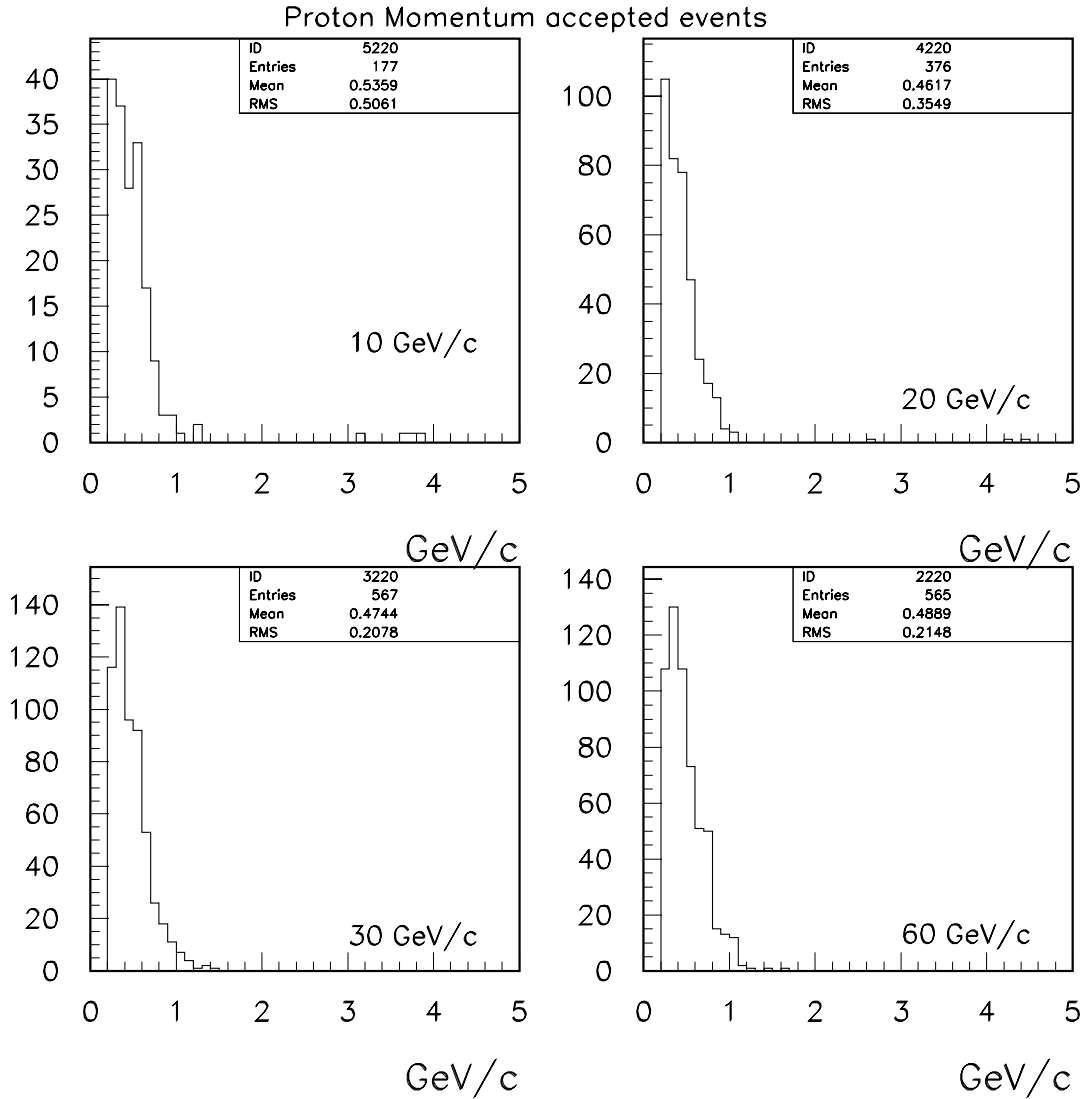


FIG. 14: Momentum spectrum of accepted protons for incident  $K^-$  momenta of 10 GeV/c, 20 GeV/c, 30 GeV/c and 60 GeV/c for the process  $K^- p \rightarrow p K_L^0 \pi^-$ .

- [5] DPMJET3.0-4 is a program written by S. Roesler, R. Engel and J. Ranft.
- [6] R. Raja, Ph.D Thesis, Cavendish laboratory (1975).
- [7] David. R. .Ward, Ph.D Thesis, Cavendish laboratory (1976).
- [8] J. Whitmore, Phys. Reports 1973.

2006/05/19 13.51

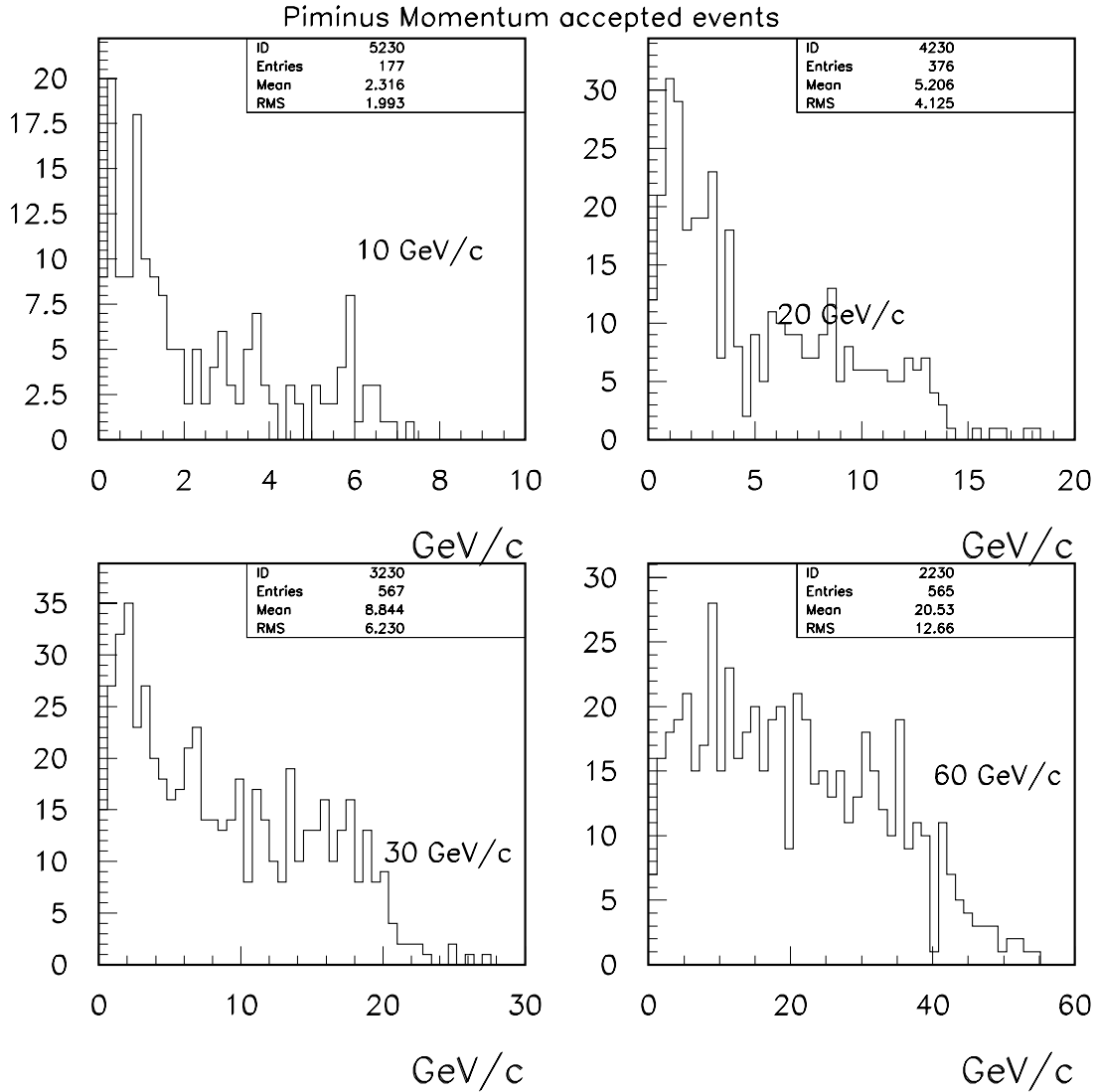


FIG. 15: Momentum spectrum of accepted  $\pi^-$  particles for incident  $K^-$  momenta of 10 GeV/c, 20 GeV/c, 30 GeV/c and 60 GeV/c for the process  $K^- p \rightarrow p K_L^0 \pi^-$ .

2006/05/20 17.06

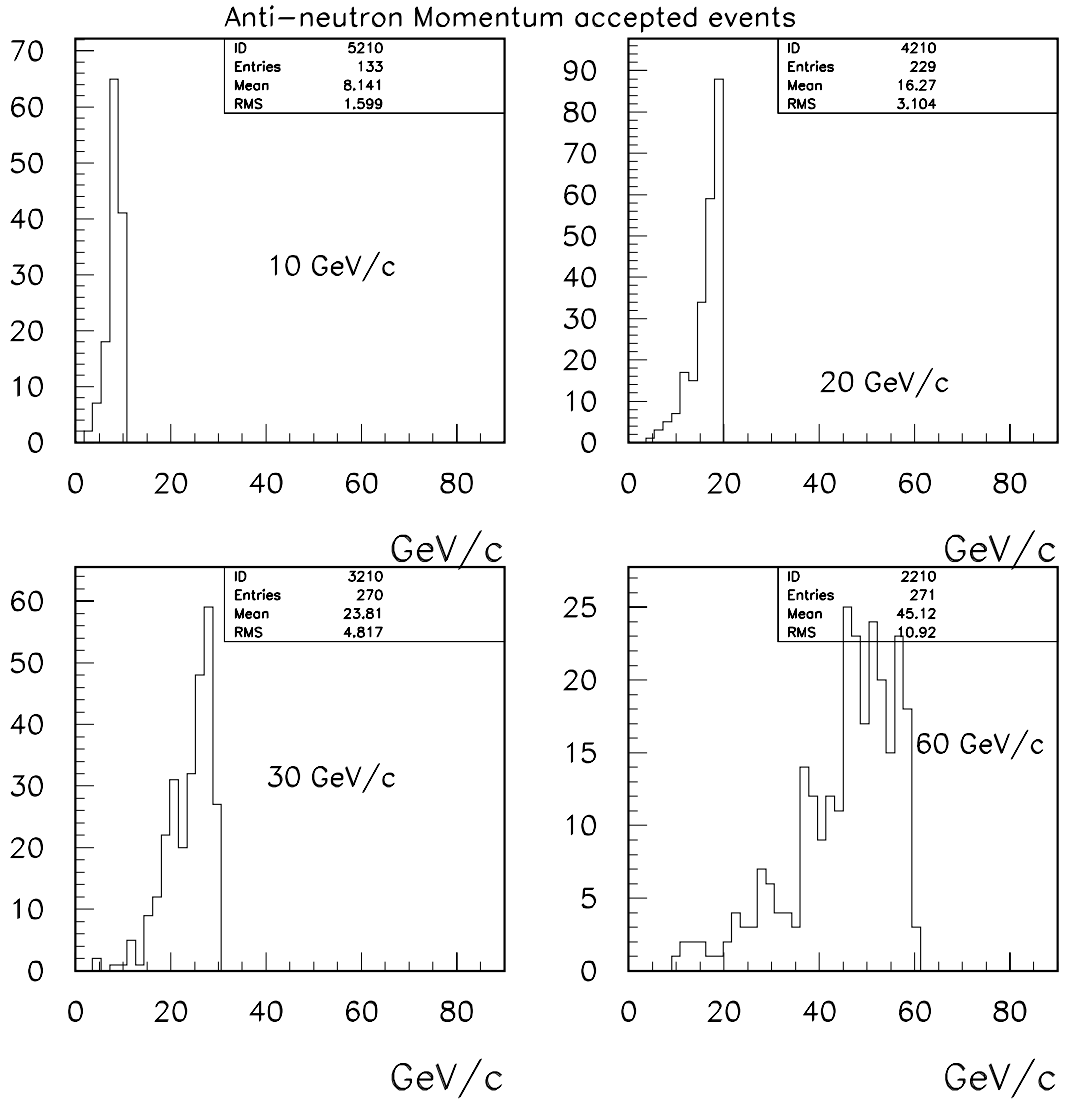


FIG. 16: Momentum spectrum of accepted anti-neutrons for incident anti-proton momenta of 10 GeV/c, 20 GeV/c, 30 GeV/c and 60 GeV/c for the process  $\bar{p}p \rightarrow p\bar{n}\pi^-$ .

2006/05/20 17.06

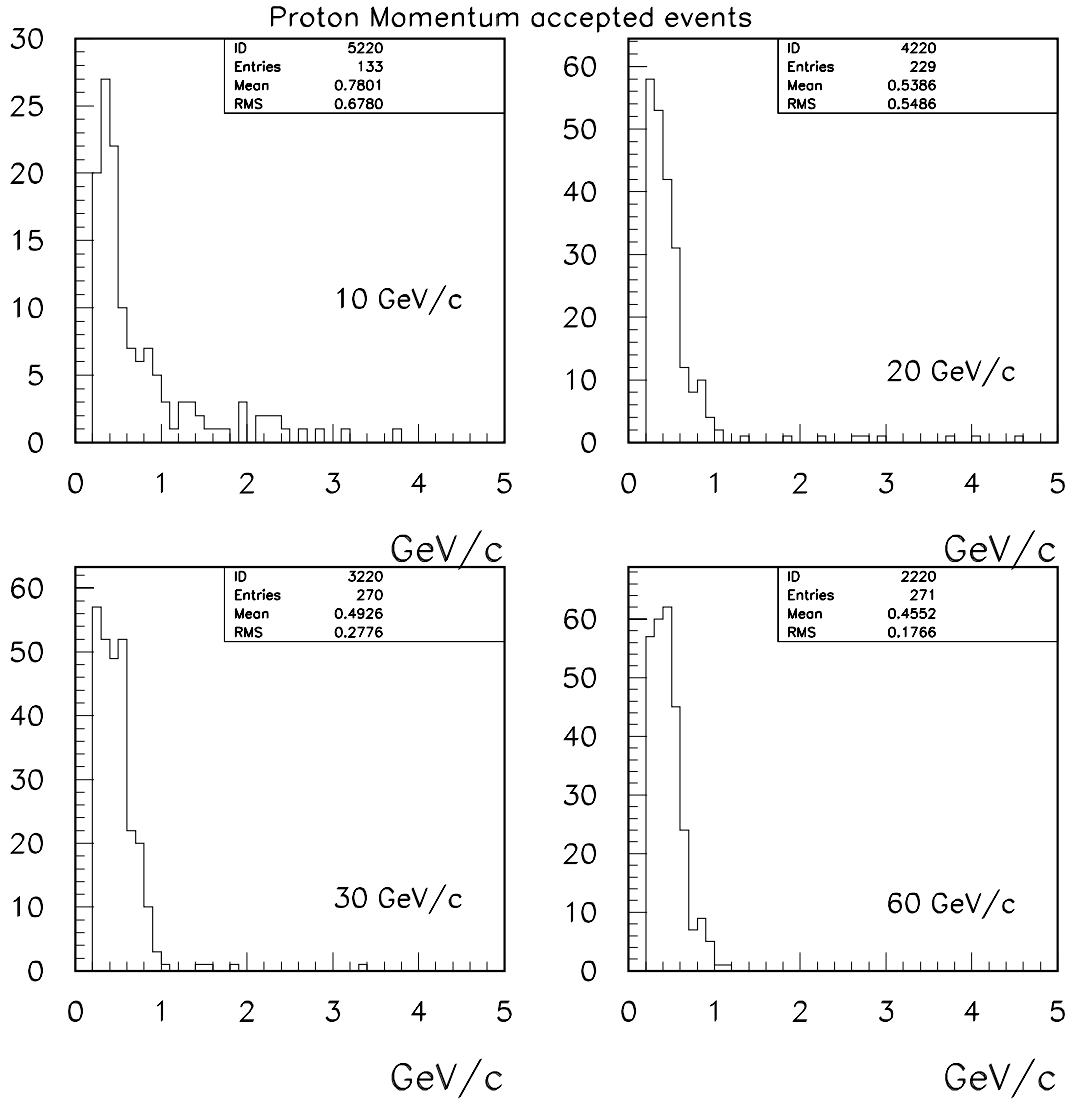


FIG. 17: Momentum spectrum of accepted protons for incident anti-proton momenta of 10  $\text{GeV}/c$ , 20  $\text{GeV}/c$ , 30  $\text{GeV}/c$  and 60  $\text{GeV}/c$  for the process  $\bar{p}p \rightarrow p\bar{n}\pi^-$ .

2006/05/20 17.06

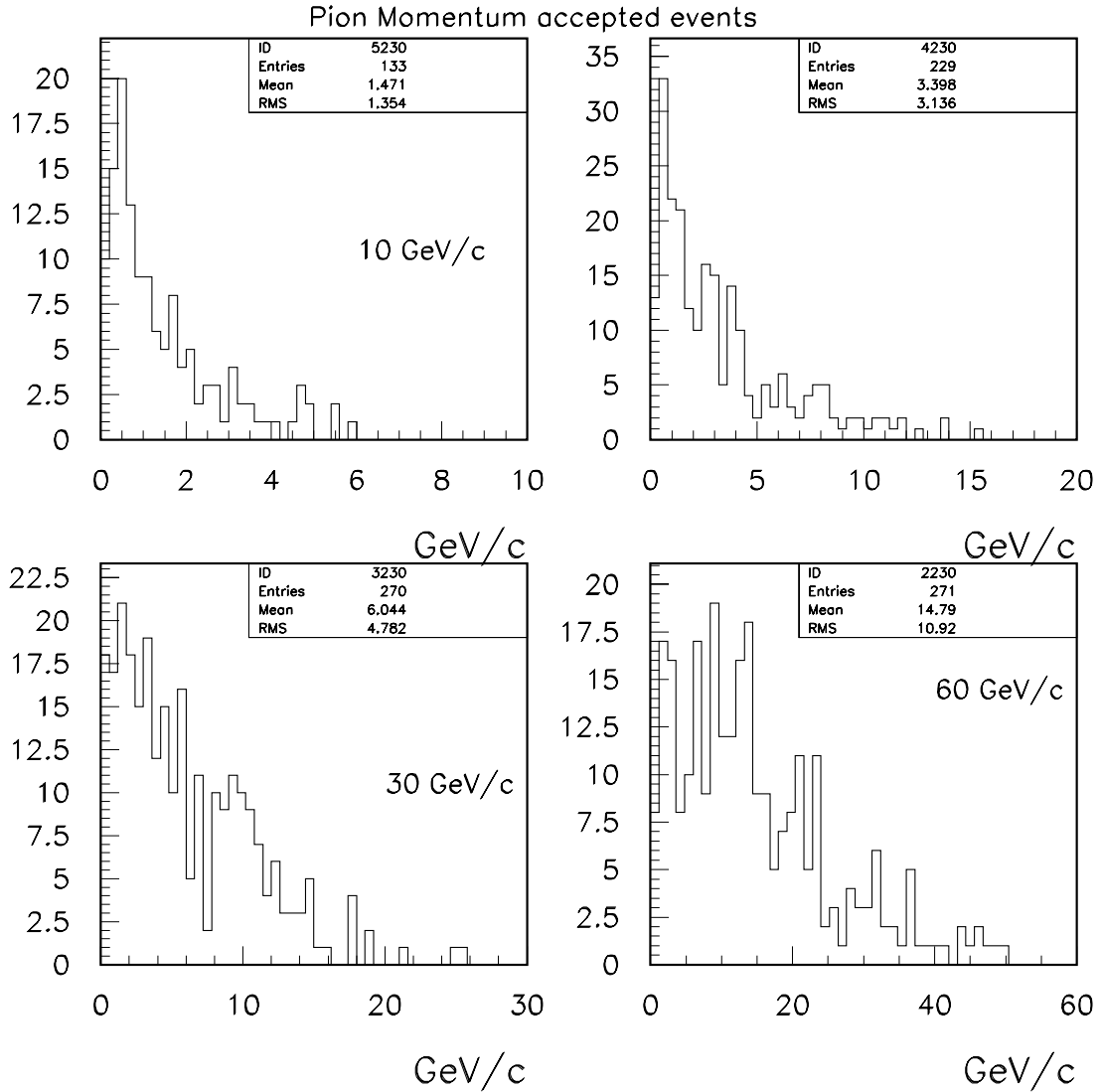


FIG. 18: Momentum spectrum of accepted  $\pi^-$  particles for incident anti-proton momenta of 10 GeV/c, 20 GeV/c, 30 GeV/c and 60 GeV/c for the process  $\bar{p}p \rightarrow p\bar{n}\pi^-$ .